# Enhancement of band gap and electrical conductivity properties of $TiO_2$ nanowire by Ni with hydrothermal method


Mahamasuhaimi Masae[a, c, *], Witthaya Sririkun[a], Peerawas Kongsong[b]

[a] Department of Industrial Engineering, Faculty of Engineering,
Rajamangala University of Technology Srivijaya, Songkhla, 90000 Thailand
[b] Department of Materials Engineering, Faculty of Engineering and Architecture,
Rajamangala University of Technology Isan, Nakhon Ratchasima, 30000 Thailand
[c] Fiber and Textile Research Unit, Faculty of Engineering, Rajamangala University of Technology Srivijaya,
Songkhla, 90000 Thailand

***Corresponding Author:** susumeme1983@yahoo.com

**Received:** 1 May 2021 | **Revised:** 25 May 2021 | **Accepted:** 1 December 2021 | **Available online:** 1 January 2022

## Abstract

Nickel doped Titanium dioxide phase B nanowires (Ni/$TiO_2$(B) NWs) were successfully fabricated by a hydrothermal method and characterized by XRD, FE-SEM, UV-vis and XPS spectroscopy. The FE-SEM images of the surface morphology showed that the size of nickel doped $TiO_2$(B) phase crystal was small (19 – 29 nm). The results indicated that the uniform Ni doped $TiO_2$(B) nanowires with a length of about 5 µm and an average diameter of about ~204.80 nm were produced. The result also showed composite with 4 mol% Ni doped $TiO_2$(B) NWs phase exhibited optimum photocatalytic activity for the synergeric effects of electrical conductivity and band gap energy. The properties study of Ni/$TiO_2$(B) NWs leading to a new applications of high-performance materials as solar cells, electronics batteries and many other applications.

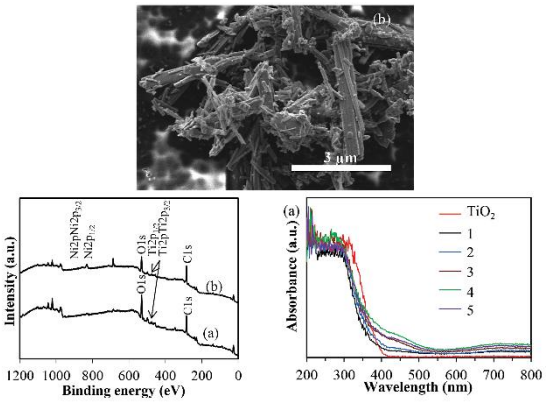


**Keywords:** $TiO_2$(B) nanowire; Hydrothermal; Ni doped $TiO_2$



## Introduction

The substance that is photoreactive, nontoxic and relatively low cost is titanium dioxide ($TiO_2$) catalyst [1]. The crystal types occur in 3 different phases: anatase, rutile, brookite and $TiO_2$(B). A lot of research works about anatase has been done because of its small crystal size. $TiO_2$(B)'s structure is less compact than that of other forms $TiO_2$ and $TiO_2$(B) is rarely found in nature. The three widely known crystallographic forms are anatase and rutile (tetragonal), brookite (orthorhombic) and $TiO_2$(B), as a metastable monoclinic modification of $TiO_2$ [2]. The structure of $TiO_2$(B) ($a$ = 12.16 Å, $b$ = 3.74 Å, $c$ = 6.51 Å, $\beta$ = 107.29º), also called monoclinic $TiO_2$. $TiO_2$(B)'s structure was first synthesized in 1980. The dehydration of layered or tunnel-structured hydrogen titanate are called the $TiO_2$(B) phase which is metastable polymorph formed [2]. The $TiO_2$(B) phase has tunnel structure and not high density. The $TiO_2$(B) phase may find use in energy storage applications [3]. Some hydrothermally synthesized $TiO_2$(B) nanowire ($TiO_2$(B) NWs) properties have been reported [4, 5]. Furthermore, these studies are achieved to apply these catalyst in the life applications. These study, a novel nickel (Ni) doped $TiO_2$(B) phase nanowires composite powder synthesis by hydrothermal method is described. $TiO_2$(B) has many applications, such as photo reactivity, nontoxicity,

semiconducting, energy storage and antibacterial activities [5, 6]. Monoclinic titania, commonly named $TiO_2$(B) phase (a metastable polymorph of titanium dioxide), has a relatively open structure with significant voids and continuous channels, facilitating lithium intercalation and leading to excellent electrochemical properties [7]. $TiO_2$(B) and Ni are value low cost functional materials. Consequently, they have with a having a huge extent of applications, such as electrochemical, catalyst supports, photocatalysis, lithium ion batteries, electrodes for solar cells and electrochromic applications [3, 6 – 10]. The titanium dioxide doped nickel composite has been used for a variety of applications. The nickel element has use in hydrogen fuel cell applications. The nickel doped Strontium (Sr) can be used in water splitting to make hydrogen for energy production [10]. The $Ni^{2+}$ is easily substituted into the $TiO_2$ lattice and creates an impurity energy level. The energy of impurity would lead to a decreased band gap and response of visible light for $TiO_2$ photocatalyst. For conductivity, at low frequency, the resistivity and grain boundary of Ni doped $TiO_2$ with high an impurity energy level effect on the conductivity that would apply lower energy to exchange electron between ions at grain boundary than pure $TiO_2$. Then, Conductivity of Ni doped $TiO_2$ is high. [11, 12]. Using a hydrothermal process with temperature at 120 °C or higher put the mixture solution in stronger KOH or NaOH will appear in the formation of solid titanium dioxide nanowires or long nanofibers. These conditions make the normal unidirection crystal growth becoming preferential. Because of its high surface area, the nanotube structure is attractive. However, anatase phase particles can be created from the structure of titanate nanotubes with free-alkali ions because it is typically unstable at high temperatures (at ~500 °C) [4, 5, 13].

These $TiO_2$(B) NWs composites by preparation with hydrothermal system and characterization will be shown in detail. We prepared the Ni/$TiO_2$(B) NWs using the hydrothermal method. Crystallization, surface microstructure optical properties, electrical conductivities and the photocatalytic properties of the powders were characterized.

## Materials and Methods

*Synthesis of Ni/$TiO_2$(B) NWs by Hydrothermal Method*

Titanium dioxide nanopowder Degussa P25 was mixed with 30 ml of 10 M sodium hydroxide (NaOH, 98%, Loba-chemie). The precursor used as a dopant (doping agent) is nickel nitrate ($Ni(NO_3)\bullet 6H_2O$) high purify which were varied to different Ni/Ti amount of 0, 1, 2, 3, 4 and 5 mol% and were sonicated for 60 min in an ultrasonic. The composite solution was moved to a 50 mL. Then heated at 220 °C for 24 h in teflon-lined autoclave container. After cooling to room temperature, the mixtures were (or the mixture was) taken out, and then were rinsed extensively with 0.10 M HCl, deionized water and followed by ethanol. Then, the mixture was calcined at 400 °C for 2 h.

*Characterization of Ni/$TiO_2$(B) NWs*

An X-ray diffractometer (X'Pert MPD, Philips) was used to characterize the X-ray diffraction (XRD) patterns. The Scherer equation (Eq. (1)) was used to determine the size of titanium crystal use equation below [14];

$$D = \frac{0.9\lambda}{\beta \cos\theta} \quad (1)$$

The symbols $D$, $\lambda$, $\beta$ and $\theta$ are the crystallite size (nm), the wavelength of the X-ray radiation ($CuK_\alpha$ = 0.15406 nm), the angle width at half maximum height, and the half diffraction angle in degree of the centroid of the peak, respectively. Morphology of the prepared powders was measured with Field emission scanning electron microscope (FE-SEM, Apreo, FEI) at acceleration voltage of 5 kV and Energy-dispersive x-ray measurements (EDX). The UV-vis spectrophotometer (UV-2401, Shimadzu) was used $BaSO_4$ as reference for observing optical properties and the band gap energy value of $TiO_2$ powder. The X-ray photoelectron spectrometer (XPS, AXIS ULTRA, Kratos analytical) was used to observe the chemical composition of the powders. The results from XPS were distinguishable with a hemispherical analyzer positioned at an angle of 45° with respect to the normal to the sample surface. To measure the DC electrical conductivity ($\sigma_{DC}$, S $cm^{-1}$) of Ni/$TiO_2$(B) NWs tablets were prepared by compression of 0.1g powder in a 10 mm diameter cylinder mold using a constant pressure. All samples were then analyzed, measuring the electrical conductivity and capacitance by LCR meter, 4285A Precision, Agilent with a frequency range of 75 kHz – 30 MHz at room temperature.

## Results and Discussion

*XRD Analysis*

The XRD patterns of $TiO_2$ powders calcined at 400 °C by hydrothermal method are presented in Fig. 1. It was

found that only the $TiO_2$(B) phase can be seen at 0 – 5 mol% Ni doping in $TiO_2$. The diffraction peaks which appear in undoped $TiO_2$ sample at $2\theta$ are 25.30, 29.20, 44.30 and 48.20 degrees, respectively. According to the JCPDS 46-1238 patterns of $TiO_2$(B) form $TiO_2$ monoclinic structure requirements [15]. P25 $TiO_2$ have anatase and rutile structure in ratio 80:20 show at $2\theta$ are 25, 37, 47 and 55 degree [16]. It was observed that the process of adding a dopant to the phase transformation has shown practically no phase change in the titanium dioxide, independent of the amount of dopant feeding and electronic structure. Moreover, Fig. 1 shows that, for various Ni species, no separate crystalline phase was detected, which suggests that Ni species were thoroughly dispersed in $TiO_2$ nanoparticles. Increasing Ni content did not show that any significant lattice deformation had occurred, which is not unexpected considering that $Ni^{2+}$ has an ionic radius similar to $Ti^{4+}$ and can also form octahedral coordination as $Ti^{4+}$ does [6].

The values of average crystal size of pure $TiO_2$(B) and Ni/$TiO_2$(B) NWs, measured from (*hkl*) planes in XRD of (101) using the Scherrer equation, were 20.67, 19.67, 29.49, 25.31, 29.53 and 29.53 nm for undoped $TiO_2$(B) and 1, 2, 3, 4 and 5 mol% Ni/$TiO_2$(B) NWs, respectively. The occurrence of Ni–O–Ti bonds in Ni-doped $TiO_2$(B) causes the grain size to decrease, which in turn impedes the growth of the crystals. Nonetheless, as the Ni concentration increases further to 1 – 2 mol%, the lattice constant values estimated increases to $a$ = 12.206 Å, and for the last three concentrations 3, 4 and 5 mol%, the lattice constant values decrease to $a$ = 11.623, 11.641 and 11.219 Å, respectively (Table 1). This shows that the substitutional $Ni^{2+}$ ions replace $Ti^{4+}$ ions and result in linear decay of the crystallite size. The lattice parameters have an effect on the crystallite size, and not different between the synthesis of undoped and Ni/$TiO_2$(B) NWs. The defect in structure is appear number of dislocations decreases. When the amount of nickel is increased with the crystal size start to increase [6].

*XPS Spectra of Ni/$TiO_2$(B) NWs*

Figure 1 (g) and (h) shows XPS spectra of $TiO_2$(B) NWs and 4 mol% Ni/$TiO_2$(B) NWs composites consist of only Ti, Ni, O and C elements and the binding energies of Ti2p, Ni2p, O1s and C1s are 456.50, 853.50, 528.50 and 283.50 eV, respectively. The O1s region of an annealed undoped $TiO_2$ show peaks at 529.70 and 531.40 eV corresponding to Ti, O and the hydroxyl group, respectively. This research, the presence of $Ti^{4+}$ in $TiO_2$ sample where found at binding energy positions corresponding to Ti2p and Ti2p lines for pure $TiO_2$(B) powders at 456.50 and 461.00 eV [14]. The binding energies of Ti2p region for the pure $TiO_2$ and $TiO_2$ doped nickel specimens were similar. Atoms existed in the forms $Ni_2O_3$ from Fig. 1(g). XPS result reveals.

*Morphology of Powder Ni/$TiO_2$(B) NWs*

Ni at 853.50 eV for Ni2p and 872.00 eV for Ni2p, and make be completely observed in Fig. 1(h). In combination from the XRD data, it may be concluded that $Ni_2O_3$ was dispersed on the surface of titania [14].

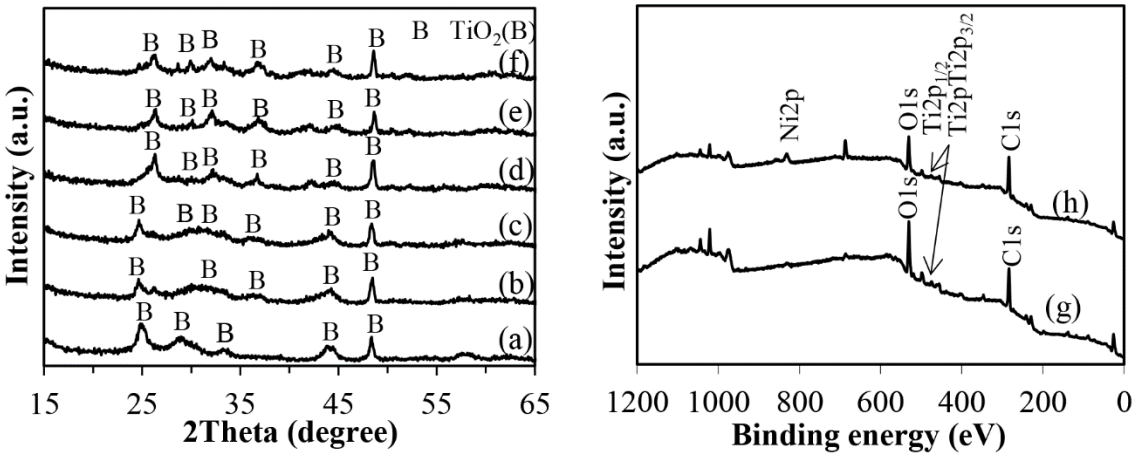


**Fig. 1** XRD patterns of pure $TiO_2$(B) NWs (a) and $TiO_2$(B) NWs at various Ni: (b) 1 mol%, (c) 2 mol%, (d) 3 mol%, (e) 4 mol%, and (f) 5 mol% Ni. XPS spectra of (g) pure $TiO_2$(B) NWs and (h) 4 mol% Ni/$TiO_2$(B) NWs.

**Table 1** Crystallite size (*D*), Lattice parameters, Cell volume (*V*), Optical properties ($E_g$), Oxygen vacancies ($E_u$) and Conductivity ($\sigma_{DC}$) and Capacitance (*G*) of pure $TiO_2$(B) and Ni/$TiO_2$(B) NWs.

| mol% Ni | *D* (nm) | Lattice parameters (Å) | | | *V* (Å$^3$) | $E_g$ (eV) | $E_u$ | $\sigma_{DC}$ (×10$^{-7}$S cm$^{-1}$) | *G* (×10$^{-11}$ F) |
|---|---|---|---|---|---|---|---|---|---|
| | | *a* | *b* | *c* | | | | | |
| $TiO_2$(B) | 20.67 | 11.647 | 3.763 | 6.488 | 284.354 | 3.37 | 2.90 | 5.50 | 8.90 |
| 1 | 19.67 | 12.206 | 3.756 | 6.687 | 306.570 | 3.50 | 2.27 | 4.50 | 3.25 |
| 2 | 29.49 | 11.823 | 3.769 | 6.422 | 286.170 | 3.50 | 2.14 | 5.20 | 4.50 |
| 3 | 25.31 | 11.623 | 3.746 | 6.725 | 292.805 | 3.45 | 1.94 | 4.50 | 6.90 |
| 4 | 29.53 | 11.641 | 3.743 | 6.406 | 279.124 | 3.33 | 1.47 | 7.50 | 7.60 |
| 5 | 29.53 | 11.219 | 3.754 | 6.397 | 269.417 | 3.35 | 1.65 | 2.20 | 6.20 |

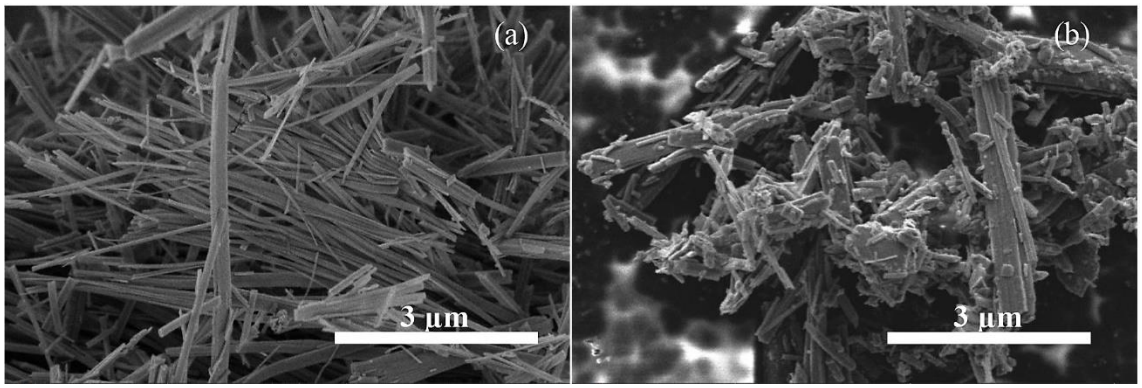


**Fig. 2** FE-SEM images of pure (a) $TiO_2$(B) NWs and (b) 5 mol% Ni doped $TiO_2$(B) NWs.

The carbon can be attributed to the remained carbon from the starting solution and the hydrocarbon from the XPS instrument itself. The structure of the composite Ni doped $TiO_2$(B) NWs powders was produced by hydrothermal method for 24 h at 220 °C and calcined at 400 °C and was characterized by FE-SEM showed in Fig. 2. The images show nanowires of the $TiO_2$(B) and the short 5 mol% $TiO_2$ nanowire that have an average diameter was increased from ~163.9 – 204.8 nm due to Ni ions might affect the expansion distortion of Ti lattice which rises particle size and morphology[8, 17]. The XRD analysis shown in Table 1. The shape and morphology of Ni/$TiO_2$(B) NWs at various Ni dosage were not found to be much different than that of undoped sample. In the hydrothermal process, $TiO_2$ particles react with NaOH solution to form sodium titanate ($Na_xTi_yO_z$). It was washed with acid to gets protonate titanate ($H_2Ti_3O_7.xH_2O$) when calcined at 400 °C to be only $TiO_2$(B) phase.

*Energy Gap Measurement*

The result in Fig. 3 presents the UV-vis spectra of $TiO_2$(B) NWs and Ni/$TiO_2$(B) NWs. The band gap energies ($E_g$) of the samples were determined and analyzed by intercept x of the linear portion of $(\alpha h\nu)^2$ as a function of E to $\alpha E = 0$ (where $E = E_g$) of following eq. (2) [18];

$$\alpha E = A'\left(E - E_g\right)^m \quad (2)$$

where $E_g$ is the band gap energy (eV) of the specimen, *A'* is the absorption constant and $\lambda$ is the wavelength of the onset of the spectrum (nm). ($E = hc/\lambda$), respectively. $m = 1/2$ for direct band gap and $m = 2$ for indirect band gap. The symbol of $\alpha$ is absorption coefficient was determined by $\alpha = A/d'$ where *A* is the measured absorbance (nm), *d'* is the thickness of specimens in UV-vis cell (0.40 cm). The data of UV-vis diffuse reflectance wavelength of nickel doped $TiO_2$ (Ni = 0, 1, 2, 3, 4 and 5 mol%) powders calcined at 400 °C for 2 h are presented in Fig. 3. It can be seen that pure

$TiO_2$(B) NWs (the undoped) and Ni/$TiO_2$(B) NWs powders (Fig. 3(a)), Ascribed to the electron transfer from the valence band (mainly formed by 2p orbitals of the oxide anions) to the conduction band (mainly formed by $t_{2g}$ peaks of Ti3d orbital of the $Ti^{4+}$ cations), are showing absorption spectra consisting of a single broad intense absorption at around 400 nm (i.e., in the UV light range) [6, 19]. From the curves it is seen that all the powder specimens have indirect band gap transitions. Table 1. shows the calculated band gap energy value ($E_g$) of these powders. From the UV-vis result it is shown that the titanium dioxide band gap energy is barely decreased, when the nickel content is increased, which corresponds to the red shift of the absorption edge measured in UV-vis spectra (Fig. 3(b)).

The value of charge transfer transitions between metal ion and the valence or conduction band of titanium dioxide can be described with these red shift lengths. Analyzing the $E_g$ and absorption edge data, the Ni/$TiO_2$(B) NWs is anticipated under visible light irradiation and the pure $TiO_2$(B) NWs to be active recombination of electron under UV irradiation [6]. The amount of nickel in titanium dioxide be effect on enrichment of visible light absorption capacity relating with the prior work [20, 21]. In addition, we describe the potential reason of band gap narrowing in $TiO_2$ with Ni doping in hydrothermal system. As reported, the Ni dopant acts as an acceptor impurity in $TiO_2$ lattice [6]. The Ni/$TiO_2$(B) NWs, the acceptor levels of Ni along with oxygen vacancies are created in the band gap of $TiO_2$.

*Electrical Properties*

Figure 4 and Table 1 show conductivity and capacitance parts as a function of frequency, respectively. The DC electrical conductivity ($\sigma_{DC}$, S $cm^{-1}$) of stoichiometric $TiO_2$(B) NWs at frequency range of 75 kHz – 30 MHz at room temperatures can be calculated by the following eq. (3) [22];

$$\sigma_{DC} = \frac{GL}{A} \tag{3}$$

Where $G$ is conductance (S), $L$ and $A$ are the thickness (cm) and the cross sectional area ($cm^2$), respectively. As shown in Fig. 4, the DC electrical conductivity increases with increasing frequency. At higher frequency range, a higher DC conductivity of the material also increases as hopping frequency of the free electrons is accelerated [23]. The DC conductivity at high frequencies is the trend required for a small polaron hopping [24 – 26]. For the host nanomaterials, conductivity showed with fairly localized vendors bound to the lattice with lattice strain i.e. with polaron conduction [24, 27, 28]. It is seen that with addition of Ni, conductivity value increases in the high frequency. The Ni addition at 4 mol% Ni/$TiO_2$(B) NWs may result in more localization of charge carriers along with mobile ions causing higher ionic conductivity because the Ni optimum dopant take the part of an acceptor impurity in $TiO_2$ lattice and the reduction of the recombination of electron-hole pairs [29].

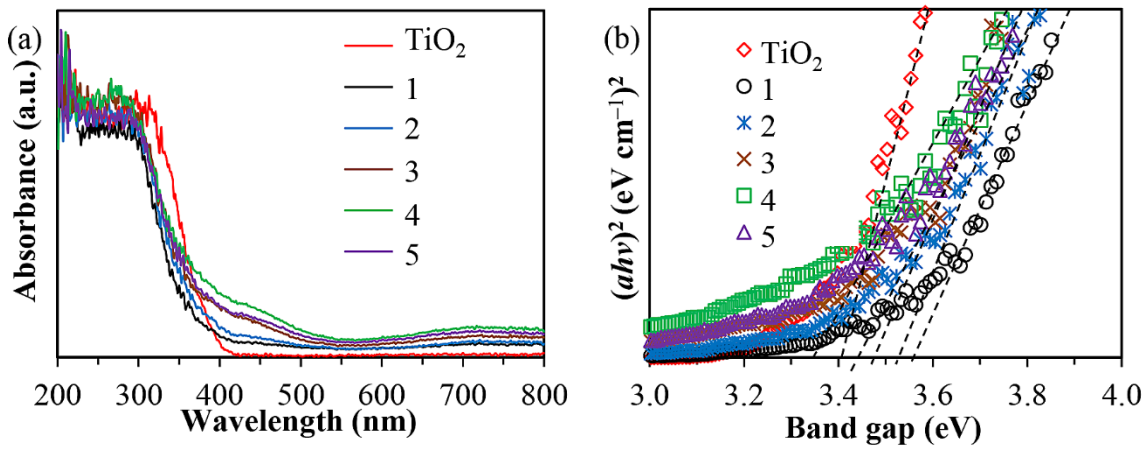


**Fig. 3** (a) UV–vis diffuse reflectance spectra and (b) the band gap energies of all samples.

Moreover, the defect concentration or oxygen vacancy concentration around grain boundaries strongly affects the motion of charge carriers suggesting the performance in electrical conductivity. The advantages of nanowire structures were validated to contribute to the enhanced electron charge separation and transportation. $TiO_2$ nanowire nanostructures have a high surface area for continuous reaction process [7]. This may be the reason for higher conductivity and strong frequency dispersion on 4 mol% Ni/$TiO_2$(B) NWs. As expected, the conductivity increases with doped Ni. The conductivity of 4 mol% Ni/$TiO_2$(B) NWs was increased by $7.50 \times 10^{-7}$ S $cm^{-1}$ compared with pure $TiO_2$ NWs is $5.50 \times 10^{-7}$ S $cm^{-1}$. The Ni crystal dispersion of $TiO_2$(B) phase particles is due to the phase action of Ni/$TiO_2$ NWs that assist in controlling the internal individual dipoles in the presence of an electric field and hence, controls the conductivity properties of the composite.

In addition, D. Zhang et al. [7] found that photovoltage spectroscopy intensity is increased with increase in Ni dopant content from an undoped up to 1.50 mol%, and then decreased. This result support the Ni (II) ions and the oxygen vacancies can is because oxygen vacancies and Ni (II) ions can go on as traps to capture the photoinduced electron. These factors result in the surface potential of Ni doped $TiO_2$ being much less than that of pure $TiO_2$ under illumination. Therefore, the inhibit electron-hole recombination make the photovoltage spectroscopy response signal increase. This is of asset to the photocatalytic reaction. While at high Ni dopant region (> 1.50 mol%), the excessive oxygen vacancies and Ni species can become the recombination centers of photoinduced electrons and holes. So, it was revealed that the intensity of photovoltage spectroscopy signal is decreased [6].

$Ni^{2+}$ has easily substituted into $TiO_2$ lattice and created an impurity energy level. The energy of impurity would lead to decreased band gap and response of visible light for $TiO_2$ photocatalyst. For conductivity, at low frequency, the resistivity and grain boundary of Ni doped $TiO_2$ with high an impurity energy level effect on the conductivity that would apply lower energy to exchange electron between ions at grain boundary than pure $TiO_2$. Then, Conductivity of Ni doped $TiO_2$ is high. [11, 12].

## Conclusion

The 4 mol% Ni doped $TiO_2$(B) NWs photocatalyst was prepared by using the hydrothermal process and exhibits a higher photoactivity than pure $TiO_2$(B) NWs. The result shows that the high amount of Ni-doped $TiO_2$(B) promotes the formation of basic sites on the surface of $TiO_2$(B). Nickel doping of $TiO_2$(B) affected in the unit cell, crystallite size and band gap energy of the $TiO_2$(B) NWs. The amount of nickel content (more than 3 mol%) can affect to larger crystal size, however the band gap energy did not linearly decrease with the increasing amount of nickel to $TiO_2$(B). The 4 mol% Ni/$TiO_2$(B) NWs is near optimal across the compositions tested, having photocatalytic activities and small crystallite size. However, while XPS measurements give evidence of such interfacial effects on the $TiO_2$(B) NWs. Further studies on 4 mol% Ni/$TiO_2$(B) NWs have a real interest, since its high electrical conductivity properties makes it desirable for making ionic batteries and electrochemical sensors.

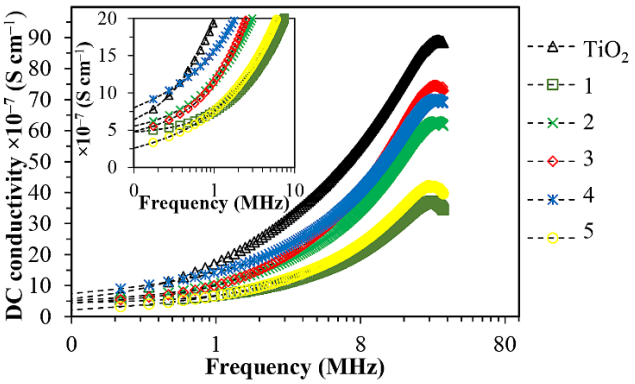


**Fig. 4** The DC electrical conductivity of $TiO_2$(B) NWs at various Ni concentrations.

## Acknowledgement

The authors would like to acknowledge Faculty of Engineering, Rajamangala University of Technology Srivijaya, Songkhla, Thailand and Fiber and Textile Research Unit for financial support of this research.

## References

[1] P. Makal, D. Das, Self-doped $TiO_2$ nanowires in $TiO_2$-B single phase, $TiO_2$-B/anatase and $TiO_2$-anatase/rutile heterojunctions demonstrating individual superiority

in photocatalytic activity under visible and UV light, Appl. Surf. Sci. 455 (2018) 1106 – 1115.

[2] Y. Zhang, Z. Jiang, J. Huang, L.Y. Lim, W. Li, J. Deng, D. Gong, Y. Tang, Y. Lai, Z. Chen, Titanate and titania nanostructured materials for environmental and energy applications: a review, RSC Adv. 5(97) (2015) 79479 – 79510.

[3] W. Wang, M. Tian, A. Abdulagatov, S.M. George, Y.C. Lee, R. Yang, Three-dimensional Ni/$TiO_2$ nanowire network for high areal capacity lithium ion microbattery applications, Nano Lett. 12(2) (2012), 655 – 660.

[4] V.N. Nguyen, N.T. Nguyen, P.H. Nguyen, Hydrothermal synthesis of Fe-doped $TiO_2$ nanostructure photocatalyst, Adv. Nat. Sci.: Nanosci. Nanotechnol. 2(3) (2011) 035014.

[5] S. León-Ríos, R. Espinoza González, S. Fuentes, E. Chávez Ángel, A. Echeverría, A.E. Serrano, C.S. Demergasso, R.A. Zárate, One-Dimensional $TiO_2$-B Crystals Synthesised by Hydrothermal Process and Their Antibacterial Behaviour on Escherichia coli, J. Nanomater. 2016 (2016) 1 – 8.

[6] I. Ganesh, A.K. Gupta, P.P. Kumar, P.C. Sekhar, K. Radha, G. Padmanabham, G. Sundararajan, Preparation and characterization of Ni-doped $TiO_2$ materials for photocurrent and photocatalytic applications, Sci. World J. 2012 (2012) 1 – 16.

[7] H.Y. Wu, M.H. Hon, C.Y. Kuan, C. Leu, Synthesis of $TiO_2$(B)/$SnO_2$ composite materials as an anode for lithium-ion batteries, Ceram. 41(8) (2015) 9527 – 9533.

[8] D. Zhang, Chemical synthesis of Ni/$TiO_2$ nano-photocatalyst for UV/visible light assisted degradation of organic dye in aqueous solution, J. Sol-Gel Sci. Technol. 58(1) (2011) 312 – 318.

[9] M.E. Olya, A. Pirkarami, M. Soleimani, M. Bahmaei, Photoelectrocatalytic degradation of acid dye using Ni-$TiO_2$ with the energy supplied by solar cell: mechanism and economical studies, J. Environ. Manage. 121 (2013) 210 – 219.

[10] W.T. Chen, A. Chan, D. Sun-Waterhouse, T. Moriga, H. Idriss, G.I. Waterhouse, Ni/$TiO_2$: A promising low-cost photocatalytic system for solar $H_2$ production from ethanol-water mixtures, J. Catal. 326 (2015) 43 – 53.

[11] S. Ahmad W. Khan, A. Raushan, Synthesis and characterization of Ni doped $TiO_2$ nanoparticles by Sol-Gel method, In Conf.: Int. Conf. on Advanced Materials for Power Engineering At: MGU. (2015).

[12] P. Soni, V.V.S. Murty, K.K. Kushwaha, The effect of $Ni^{2+}$ ions on energy band gap of $TiO_2$ nanoparticles for solar cell applications. J. Nanosci. Nanoeng. Appl. 8(2) (2018) 69 – 74.

[13] A. Byeon, M. Boota, M. Beidaghi, K.V. Aken, J.W. Lee, Y. Gogotsi, Effect of hydrogenation on performance of $TiO_2$(B) nanowire for lithium ion capacitors, Electrochem. Commun. 60 (2015) 199 – 203.

[14] L. Sikong, M. Masae, K. Kooptarnond, W. Taweepreda, F. Saito, Improvement of hydrophilic property of rubber dipping former surface with Ni/B/$TiO_2$ nano-composite film, Appl. Surf. Sci. 258(10) (2012) 4436 – 4443.

[15] J. Cui, D. Sun, S. Chen, W. Zhou, P. Hu, H. Liu, Z. Huang, Enhancement of selective determination of the perfect match and mismatch of single nucleobases with a biosensing electrode based on surface-coarsened anatase $TiO_2$ nanobelts, J. Mater. Chem. 21(29) (2011) 10633 – 10636.

[16] K.F. He, E.N. Xu, Y. Liu, W.P. Chen, Hydrogenation of nano-structured $TiO_2$ photocatalyst through an electrochemical method, J. Nanosci. Nanotechnol. 15(1) (2015) 303 – 308.

[17] P. Hermawan, H.D. Pranowo, I. Kartini, Physical characterization of Ni(II) doped $TiO_2$ nanocrystal by sol-gel process, Indo. J. Chem. 11(2) (2011) 135 – 139.

[18] B. Xu, J. Ding, L. Feng, Y. Ding, F. Ge, Z. Cai, Self-cleaning cotton fabrics via combination of photocatalytic $TiO_2$ and superhydrophobic $SiO_2$, Surf. Coat. Technol. 262 (2015) 70 – 76.

[19] N.S. Begum, H.F. Ahmed, K.R. Gunashekar, Effects of Ni doping on photocatalytic activity of $TiO_2$ thin films prepared by liquid phase deposition technique, Bull. Mater. Sci. 31(5) (2008) 747– 751.

[20] M.M. Haque, A. Khan, K. Umar, N.A. Mir, M. Muneer, T. Harada, M. Matsumura, Synthesis, characterization and photocatalytic activity of visible light induced Ni-doped $TiO_2$, Energy Environ. Focus. 2(1) (2013) 73 – 78.

[21] G. Cai, J. Tu, D. Zhou, L. Li, J. Zhang, X. Wang, C. Gu, Constructed $TiO_2$/NiO core/shell nanorod array for efficient electrochromic application, J. Phys. Chem. C. 118(13) (2014) 6690 – 6696.

[22] N. Sriharan, N. Muthukumarasamy, T.S. Senthil, Preparation and characterization of $Al_2O_3$ doped $TiO_2$ nanocomposites prepared from simple sol-gel method, Z. Phys. Chem. 230(12) (2016) 1745 – 1758.

[23] R. Chang, Y. Tian, Y. Wang, J. Qin, pH-responsive vesicles with tunable membrane permeability and hydrodynamic diameters from a cross-linkable amphiphilic block copolymer, Nanomater. Nanotechnol. 6(6) (2016) 1 – 6.

[24] S. Sagadevan, K. Pal, P. Koteeswari, A. Subashini, Synthesis and characterization of $TiO_2$/graphene oxide nanocomposite, J. Mater. Sci.: Mater. Electron. 28(11) (2017) 7892 – 7898.

[25] A.N. Patil, M.G. Patil, K.K. Patankar, V.L. Mathe, R.P. Mahajan, S.A. Patil, Dielectric behaviour and ac conductivity in $CuxFe_{3-x}O_4$ ferrite, Bull. Mater. Sci. 23(5) (2000) 447 – 452.

[26] S. Kurien, S. Sebastian, J. Mathew, K.C. George, Structural and electrical properties of nano–sized magnesium aluminate, Indian J. Pure Appl. Phys. 42 (2004) 926 – 933.

[27] C.R. Indulal, R. Raveendran, Synthesis, characterization and dielectric studies of cerium phospho iodate and cadmium doped cerium phospho iodate in nano form, Indian J. Pure Appl. Phys. 48 (2010) 121 – 126.

[28] M. Raghasudha, D. Ravinder, P. Veerasomaiah, Influence of $Cr^{3+}$ ion on the dielectric properties of nano crystalline Mg-Ferrites synthesized by citrate-gel method, Mater. Sci. Appl. 4(7) (2013) 432 – 438.

[29] H.L. Qin, G.B. Gu, S. Liu, Preparation of nitrogen-doped titania with visible-light activity and its application, C. R. Chim. 11(1 – 2) (2008) 95 – 100.